Acta Cryst. (1996). B52, 982–988

Ab Initio Powder Structure Determination and Thermal Behavior of a New Lead(II) Phenylphosphonate, $Pb(O_3PC_6H_5)$

A. CABEZA,[a] M. A. G. ARANDA,[a]* M. MARTINEZ-LARA,[a] S. BRUQUE[a] AND J. SANZ[b]

[a]*Departamento de Química Inorgánica, Cristalografía y Mineralogía, Universidad de Málaga, 29071 Málaga, Spain, and* [b]*Instituto de Ciencia de Materiales, CSIC, Cantoblanco, 28049 Madrid, Spain*

(*Received 26 December 1995; accepted 22 May 1996*)

Abstract

The crystal structure of $Pb(O_3PC_6H_5)$ has been solved from X-ray powder diffraction data. Crystal data: triclinic, $a = 13.6907(5)$, $b = 9.3327(4)$, $c = 7.0432$ Å, $\alpha = 106.188(3)$, $\beta = 94.927$, $\gamma = 96.977°$, $V = 851.04(8)$ Å^3, space group $P\bar{1}$ and $Z = 4$. Initial positional parameters for Pb atoms were obtained from direct methods using 556 structure factors in the 2θ range 9–63°. All remaining non-H atoms were located from successive difference-Fourier maps. The final agreement factors were $R_{wp} = 0.055$, $R_p = 0.042$ and $R_F = 0.017$. There are 22 atoms in the asymmetric part of the unit cell and 66 positional parameters have been refined with the help of soft constraints. The lead coordination environment is irregular due to a marked inert pair effect. The three-dimensional structure of this organic–inorganic compound is layered with inorganic layers built up from CPO_3 tetrahedra and PbO_6 units. ^{31}P MAS and CP-MAS (cross-polarization magic-angle spinning) NMR studies have been carried out to confirm the triclinic symmetry with two independent structural units. In optimum conditions two ^{31}P resonance signals are observed, indicating that there are two crystallographically independent P atoms with closely similar environments. The thermal behavior of this material has been studied and the thermal decomposition products identified.

1. Introduction

Metal phosphonates are very useful for ordering molecules into lamellar structures (Thompson, 1994). These compounds are hybrid (organic–inorganic) materials and usually consist of alternating inorganic and organic layers. They can be prepared as polycrystalline solids, thin films or membranes, depending upon the applications. Nowadays, there is a great deal of work in metal phosphonates due to their interesting physical and chemical properties. These compounds can act as host materials in intercalation reactions (Johnson *et al.*, 1989; Cao & Mallouk, 1991; Zhang, Scott & Clearfield, 1993) and if properly functionalized may serve as catalysts (Segawa, Sugiyama & Kurusu, 1990; Cheng & Clearfield, 1986), ionic and electronic conductors (Alberti, Casciola, Palombari & Peraio, 1992), and ion exchangers (Alberti, Costantino & Giovagnotti, 1979; Dines & Griffith, 1983; Kullberg & Clearfield, 1989).

To understand these properties it is vital to know their crystal structures precisely. Unfortunately, most of these compounds do not grow as single crystals, hence, it is necessary to use powder diffraction methodology. Although the framework of these materials is usually lamellar, most have new structures. In recent years it has been shown that crystal structures can also be determined *ab initio* (without any prior structural knowledge) by powder diffraction (Rudolf, Saldarriaga & Clearfield, 1986; Cheetham, 1993).

On the other hand, there are many divalent metal phosphonates reported in the literature (Cunningham, Hennelly & Deeney, 1979; Martin, Squattrito & Clearfield, 1989). There is an isostructural series of compounds, with the chemical formula $M^{II}(O_3PC_6H_5).H_2O$ (M = Mg, Mn, Cd, Co, Zn), which crystallize in the orthorhombic system. The structure is built up of inorganic layers of composition $M(O_3P)$, with the phenyl groups pointing into the interlamellar space (above and below the inorganic layer). There are only van der Waals interactions between these organic bilayers (Cao, Lee, Lynch & Mallouk, 1988). The metal cations are in an octahedral environment bonded to five oxygens of the phosphonate groups and to the oxygen of the water molecule.

There are other divalent metals that crystallize with different structures. For instance, $Ca(O_3PCH_3).H_2O$ is also layered, but the atomic arrangement in the inorganic layer is different, as the environment of Ca atoms is a distorted pentagonal bipyramid of oxygens (Cao, Lynch, Swinnea & Mallouk, 1990). $Ca(HO_3PC_6H_{13})_2$ is also layered, but the stoichiometry differs as this compound is a hydrogen phosphonate resulting in a metal:phosphorus ratio of 1:2 (Cao, Lynch, Swinnea & Mallouk, 1990). $M(HO_3PC_6H_5)_2$(M = Ba,Pb) are isostructural compounds (Poojary *et al.*, 1996) with layered structures similar to those of $Zr(HPO_4)_2.H_2O$ (Clearfield & Smith, 1969; Troup & Clearfield, 1977) and $Zr(O_3PC_6H_5)_2$

(Poojary, Hu, Campbell & Clearfield, 1993). The structure of the barium compound was determined from single crystal data, which was then used as a starting model for the Rietveld refinement of the powder diffraction data of the lead analog.

It is important to underline that although most of the divalent metal phosphonates are layered, there are examples of three-dimensional structures. For instance, β-$Cu(O_3PCH_3)$ crystallizes in the trigonal system with the copper cations in distorted tetragonal pyramids of oxygens. This structure is three-dimensional with channels running along the c axis. The phenyl groups point to the interior of these channels, resulting in hydrophobic tunnels (Le Bideau, Payen, Palvadeau & Bujoli, 1994; Poojary, Zhang & Clearfield, 1994; Poojary, Grohol & Clearfield, 1995).

We are currently carrying out a detailed study of some metal phenylphosphonates (Cabeza, 1995). In this paper we report the synthesis, crystal structure and thermal behavior of a different form of lead phenylphosphonate, $Pb(O_3PC_6H_5)$.

2. Experimental

2.1. *Synthesis*

Lead(II) phenylphosphonate was obtained by slow addition of a solution of phenylphosphonic acid (1 M) over a solution of lead(II) acetate (0.1 M) to a final P:Pb molar ratio of 1:3. The precipitate was refluxed for 1 week. The white powder was filtered, washed with water and air dried. Single crystals were not obtained. The P:Pb ratio in the initial solution is a critical parameter in the synthetic process; if the phosphorus content increases, a mixture of phases is obtained. The solids isolated for P:Pb ratios of 1:1, 3:1 and 6:1 were a mixture of $Pb(O_3PC_6H_5)$ and $Pb(HO_3PC_6H_5)_2$. For P:Pb ratios higher than 8:1 lead(II) phenylhydrogenphosphonate, $Pb(HO_3PC_6H_5)_2$, is obtained as a single phase (Poojary *et al.*, 1996; Cabeza, 1995).

The sample was dissolved in a solution containing an equimolar ratio of HNO_3 (67% w/w) and H_2O_2 (30% w/w). Then, the lead content was determined by atomic absorption spectroscopy. Carbon and hydrogen contents were determined by elemental chemical analysis in a Perkin–Elmer 240 analyzer. The phosphorus content was deduced from the carbon percentage found, assuming a C:P molar ratio of 6:1. The results were: Pb 56.0, P 8.48, C 19.72, H 1.42; calculated for $PbO_3PC_6H_5$: Pb 57.02, P 8.53, C 19.83, H 1.38%.

2.2. *X-ray data collection*

Thermal analysis (TGA and DTA) was carried out in air on a Rigaku Thermoflex apparatus at the heating rate 10 K min^{-1} with calcined Al_2O_3 as reference. X-ray powder diffraction data were collected with a Siemens D-501 automated diffractometer using graphite-monochromated Cu $K\alpha$ radiation.* The powder pattern of the sample showed a very high proportion of the preferred orientation as the microcrystals have a thin plate shape. Hence, we have adapted a standard method to reduce it as much as possible (Morris *et al.*, 1977). This method dilutes and blends the sample with spherical particles which can prevent the sample from becoming oriented. Originally, the authors used finely ground silica gel. We have used Cab-osil M-5 (from Fluka), which are spherical particles of silica with approximate size ranging between 12 and 45 nm. The Cab-osil:sample weight ratio has to be optimized and 15% Cab-osil was a good value. This method allowed us to press the sample to obtain a flat surface without the highly preferred orientation. Cab-osil does not add any diffraction peaks and the background is only slightly increased in the region 20–30° (2θ). Experimental conditions of the pattern collected for the structural study of $Pb(O_3PC_6H_5)$ are given in Table 1. The data were transferred to a VAX computer for Rietveld analysis by the *GSAS* suite of programs (Larson & Von Dreele, 1987).

Table 1. *Some data for the Rietveld refinement of* $Pb(O_3PC_6H_5)$

Wavelength	Cu $K\alpha_{1,2}$
Pattern range, 2θ (°)	9–100
Step size, 2θ (°)	0.03
Counting time(s)	15
X-ray tube intensity (mA)	22
X-ray tube voltage (kV)	40
a (Å)	13.6907 (5)
b (Å)	9.3327 (4)
c (Å)	7.0432 (3)
α (°)	106.188 (3)
β (°)	94.927 (3)
γ (°)	96.977 (2)
V (Å^3)	851.04 (8)
Preferred orientation factor along [100]	0.868 (2)
No. of reflections*	2960
No. of geometric observations	42
P—O distances (Å)	1.53 (1) × 6
P—C distances (Å)	1.80 (1) × 2
C—C distances, consecutive (Å)	1.40 (1) × 12
O—O distances in PO_3 (Å)	2.55 (2) × 6
O—C distances in CPO_3 (Å)	2.73 (2) × 6
C—C distances (alternate) (Å)	2.42 (2) × 10
No. of structural parameters	69
No. of overall parameters	16
R_{wp}	0.055
R_p	0.042
R_F	0.017

* Taking into account both Cu $K\alpha_{1,2}$ wavelengths.

* The numbered intensity of each measured point on the profile has been deposited with the IUCr (Reference: DU0407). Copies may be obtained through The Managing Editor, International Union of Crystallography, 5 Abbey Square, Chester CH1 2HU, England.

Table 2. *Powder diffraction data for* $Pb(O_3PC_6H_5)$

d_{calc} (Å)	d_{obs} (Å)	$h\,k\,l$	$I_o/I_m \times 100$
13.535	13.46	1 0 0	100
8.843	8.856	0 1 0	1.8
7.970	7.993	1 $\bar{1}$ 0	1.8
6.716, 6.732	7.732	0 0 1, 2 0 0	11.4
6.332	6.330	1 0 $\bar{1}$	0.8
5.800	5.802	2 $\bar{1}$ 0	1.2
5.695	5.705	1 $\bar{1}$ 1	1.1
5.081	5.081	2 0 1	3.5
4.714	4.711	1 $\bar{1}$ $\bar{1}$	4.2
4.614	4.621	2 1 $\bar{1}$	5.8
4.404	4.401	1 $\bar{2}$ 0	2.3
4.240	4.239	1 1 1	6.6
4.031, 4.023	4.023	1 2 $\bar{1}$, 1 2 0	2.4
3.9850	3.9834	2 $\bar{2}$ 0	2.6
3.6706	3.6718	3 1 $\bar{1}$	4.1
3.6435	3.6422	3 $\bar{1}$ 1	3.4
3.5926	3.5901	2 1 1	1.7
3.4612	3.4636	2 2 0	4.8
3.4214	3.4217	3 $\bar{2}$ 0	2.8
3.3580	3.3608	0 0 2	4.1
3.3216, 3.3189	3.3190	1 $\bar{2}$ 1, 4 $\bar{1}$ 0	5.0
3.2792	3.2806	0 2 1	1.8
3.1542	3.1394	0 2 $\bar{2}$	5.6
3.7064, 3.0659, 3.0658	3.0703	1 2 $\bar{2}$, 1 2 1, 1 $\bar{2}$ 2	3.6
2.9796, 2.9757	2.9762	4 1 $\bar{1}$, 1 3 0	4.3
2.9339	2.9361	3 2 0	4.8
2.900, 2.8987	2.9007	4 $\bar{2}$ 0, 3 $\bar{2}$ 1	2.8
2.8655, 2.8649, 2.8649	2.8644	2 $\bar{3}$ 0, 2 2 $\bar{2}$, 3 0 $\bar{2}$	7.6
2.0851	2.8014	2 1 $\bar{2}$	1.0
2.7650	2.7623	2 2 1	0.9
3.3239, 3.3242	2.6916	5 $\bar{1}$ 0, 5 0 0	5.9
2.6567	2.6559	3 $\bar{3}$ 0	1.8
2.6142, 2.6117	2.6108	5 0 $\bar{1}$, 3 $\bar{1}$ $\bar{2}$	1.5
2.5841	2.5845	4 $\bar{2}$ $\bar{1}$	1.4
2.5404	2.5378	4 0 $\bar{2}$	2.9
2.5007	2.5008	4 2 0	2.2
2.3987, 2.3968	2.3952	5 0 1, 1 $\bar{2}$ $\bar{2}$	0.9
2.3593, 2.3570	2.3488	5 $\bar{2}$ 1, 2 $\bar{2}$ $\bar{2}$	0.7
2.3397, 2.3394, 2.3387	2.3353	1 1 $\bar{3}$, 1 3 1, 0 1 $\bar{3}$	2.8

2.3. *X-ray data analysis*

The powder diffraction pattern of $Pb(O_3PC_6H_5)$ (Table 2) was auto-indexed using *TREOR*90 (Werner, Eriksson & Westdahl, 1985) and *DICVOL*91 (Boultif & Loüer, 1991) with KCl as internal standard. Both indexing programs gave a similar triclinic unit cell. The result was $a = 13.672(13)$, $b = 9.315(10)$, $c = 7.047(8)$ Å, $\alpha = 106.2(1)$, $\beta = 94.8(1)$, $\gamma = 97.0(1)°$, $V = 848.9(1)$ Å^3, $Z = 4$, V (non-H atom) $= 19.29$ Å^3, with figures of merit $M_{20} = 16$ (Wolff, 1968) and $F_{20} = 32$ (0.0135, 46) (Smith & Snyder, 1979).

As we could not find any structurally related compound, we attempted to solve the structure by *ab initio* procedures. The pattern decomposition option (Le Bail, Duroy & Fourquet, 1988) of the *GSAS* package (Larson & Von Dreele, 1987) was used to extract corrected structure factors from a limited region of the diffractogram ($9 < 2\theta < 63°$). The pattern was fit without any structural model by refining the overall parameters: background, unit-cell parameters, zero-point error, peak shape (pseudo-Voigt). The refinement converged to $R_{wp} = 4.3$ and $R_p = 2.9\%$; R factors are as defined by Rietveld (1969) and Larson & Von Dreele (1987). In Le Bail's method the integrated intensities are not refined in the least-squares process, but they are assigned intial values which are corrected in the next cycle. This methodology saves computing time and ensures convergence, but does not provide a standard deviation to the determined structure factors. A total of 556 reflections were used as input to the direct-methods option of the *SHELXS*86 program (Sheldrick, 1985). The positions of the two Pb atoms were derived from this method. A difference-Fourier map prepared with only these data did not reveal any other atoms.

With the positions of the two crystallographically independent Pb atoms we used the Rietveld methods again and the overall parameters obtained in the last cycle of the *ab initio* refinement. With the inclusion of these two atoms and refining only the scale factor, R_{wp} dropped to 37%. This value was further reduced to 35% by refining the preferred orientation factor along the [100] direction. At this stage, the positions of the P atoms were derived from a difference-Fourier map and R_{wp} was decreased to 26.3%. Then, another difference-Fourier map revealed some O atoms, however, to locate all the O atoms we needed to refine the positional parameters of the atoms found. At this stage we used soft constraints in the P—O bonds to avoid the structure blow up. Following this iterative process, all C atoms were also located. To keep a reasonable geometry for the CPO_3 tetrahedra and the phenyl rings we used the soft constraints given in Table 1. Initially, we used quite a high weighting factor for the soft constraints. With all the non-H atoms located (22 in the asymmetric part of the unit cell) and refining all positional parameters R_{wp} dropped to 10.3%. At this stage we decreased the value of the weighting factor of the soft constraints and also refined the overall parameters. Refining isotropic temperature factors freely resulted in some negative values. It is well known that temperature factors, for complex structures with heavy cations and medium-resolution X-ray powder data, are quite unreliable. Hence, we decided to refine an isotropic temperature factor for each Pb atom and an overall temperature factor for the remaining atoms.

Crystallographic data of the refinement of $Pb(O_3PC_6H_5)$ are given in Table 1. The last refinement converged to $R_{wp} = 5.5\%$ with a weighting factor for the soft constraints of -250. Results of the refinement are given in Table 3 and the final observed, calculated and difference profiles are given in Fig. 1. The refined bond distances and angles are shown in Table 4.

2.4. *MAS NMR data collection*

^{31}P MAS and CP-MAS NMR spectra were recorded at 161.96 MHz on a MSL-400 Bruker spectrometer. The samples were spinning in the range 4–14 kHz. MAS spectra were taken after a $\pi/2$ pulse irradiation (6 μs). The number of scans was 10 and the time interval

Table 3. *Fractional atomic coordinates and equivalent isotropic displacement parameters ($Å^2$)*

$U_{eq} = (1/3)\Sigma_i\Sigma_j U_{ij} a_i^* a_j^* \mathbf{a}_i.\mathbf{a}_j$.

	x	y	z	U_{eq}
Pb(1)	0.8999 (2)	0.9217 (3)	0.1293 (5)	0.0125 (11)
Pb(2)	0.0662 (2)	0.6751 (3)	0.4103 (4)	0.0068 (10)
P(1)	0.1225 (6)	0.1112 (11)	0.4165 (19)	0.0002 (20)
P(2)	0.0938 (6)	0.6853 (10)	0.8887 (16)	0.0002
O(11)	0.0611 (12)	0.0568 (26)	0.2091 (22)	0.0002
O(12)	0.1071 (13)	0.9891 (21)	0.5245 (32)	0.0002
O(13)	0.0820 (11)	0.2424 (19)	0.5571 (32)	0.0002
O(21)	0.0330 (13)	0.5681 (18)	0.7066 (24)	0.0002
O(22)	0.0418 (14)	0.7079 (22)	0.0763 (23)	0.0002
O(23)	0.1234 (11)	0.8351 (16)	0.8433 (22)	0.0002
C(11)	0.2528 (8)	0.1642 (16)	0.3967 (34)	0.0002
C(12)	0.3002 (10)	0.3126 (15)	0.488 (5)	0.0002
C(13)	0.3036 (12)	0.0600 (23)	0.276 (5)	0.0002
C(14)	0.4043 (10)	0.3417 (25)	0.512 (5)	0.0002
C(15)	0.4027 (14)	0.1064 (29)	0.256 (5)	0.0002
C(16)	0.4556 (9)	0.2415 (28)	0.385 (6)	0.0002
C(21)	0.2079 (7)	0.6157 (20)	0.940 (4)	0.0002
C(22)	0.2988 (8)	0.6960 (34)	0.924 (6)	0.0002
C(23)	0.2078 (12)	0.4996 (29)	0.030 (5)	0.0002
C(24)	0.3875 (8)	0.661 (4)	1.001 (6)	0.0002
C(25)	0.2961 (13)	0.471 (14)	1.119 (5)	0.0002
C(26)	0.3863 (11)	0.5395 (34)	1.082 (5)	0.0002

between successive scans 5 s. CP-MAS spectra were obtained using a standard cross-polarization pulse sequence. The Hartman–Hann condition was chosen with a rotating H_1 field of 15 G for the decoupling channel (400.13 MHz). For recorded spectra a contact time of 1 ms and a period between successive accumulations of 5 s were chosen. The number of scans was 40. In both cases the filter band width used was 60 kHz. ^{31}P spectra were recorded at room temperature and chemical shift values were given relative to that of a 85% H_3PO_4 aqueous solution.

2.5. *MAS NMR data analysis*

The line base was corrected using a fourth-order polynomium. The isotropic chemical shift value of ^{31}P components (δ_{iso}) was determined from the band whose position does not change with the spinning rate (^{31}P spectra taken at different rates).

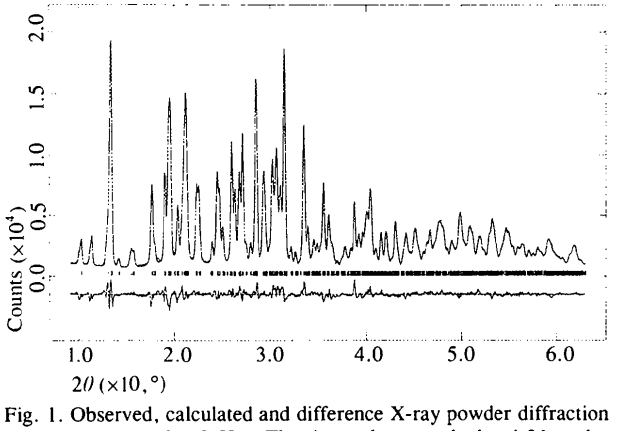

Fig. 1. Observed, calculated and difference X-ray powder diffraction profiles for $Pb(O_3PC_6H_5)$. The tic marks are calculated 2θ angles for Bragg peaks.

Table 4. *Bond distances (Å) and angles (°) for $Pb(O_3PC_6H_5)$*

Pb(1)—O(11)	2.344 (16)	Pb(2)—O(21)	2.603 (21)
Pb(1)—O(11)	2.543 (16)	Pb(2)—O(21)	2.386 (14)
Pb(1)—O(12)	2.361 (21)	P(1)—O(13)	1.539 (4)
Pb(1)—O(13)	3.028 (25)	P(1)—O(11)	1.539 (4)
Pb(1)—O(22)	2.924 (17)	P(1)—O(12)	1.541 (4)
Pb(1)—O(23)	2.288 (13)	P(1)—C(11)	1.820 (4)
Pb(2)—O(12)	2.785 (18)	P(2)—O(22)	1.530 (4)
Pb(2)—O(13)	2.264 (13)	P(2)—O(23)	1.534 (4)
Pb(2)—O(22)	2.455 (16)	P(2)—O(21)	1.531 (4)
Pb(2)—O(23)	2.985 (21)	P(2)—C(21)	1.809 (4)
O(13)—Pb(1)—O(11)	96.0 (5)	O(22)—Pb(1)—O(12)	106.3 (5)
O(13)—Pb(1)—O(11)	148.1 (6)	O(23)—Pb(1)—O(12)	80.1 (6)
O(13)—Pb(1)—O(22)	64.3 (4)	O(22)—Pb(2)—O(21)	90.6 (5)
O(13)—Pb(1)—O(23)	130.7 (6)	O(23)—Pb(2)—O(12)	62.3 (4)
O(13)—Pb(1)—O(12)	50.6 (4)	O(23)—Pb(2)—O(21)	53.2 (3)
O(11)—Pb(1)—O(11)	78.5 (5)	O(23)—Pb(2)—O(21)	122.4 (5)
O(11)—Pb(1)—O(22)	71.1 (6)	O(12)—Pb(2)—O(21)	112.9 (5)
O(11)—Pb(1)—O(23)	76.4 (7)	O(12)—Pb(2)—O(21)	157.1 (5)
O(13)—Pb(2)—O(22)	84.2 (7)	O(21)—Pb(2)—O(21)	69.5 (5)
O(13)—Pb(2)—O(23)	87.3 (6)	O(11)—P(1)—O(12)	110.0 (6)
O(13)—Pb(2)—O(12)	73.9 (5)	O(11)—P(1)—C(11)	110.7 (5)
O(13)—Pb(2)—O(21)	85.9 (7)	O(12)—P(1)—C(11)	112.1 (4)
O(13)—Pb(2)—O(21)	83.7 (6)	O(23)—P(2)—O(21)	110.9 (5)
O(22)—Pb(2)—O(23)	144.7 (5)	O(23)—P(2)—C(21)	106.5 (5)
O(22)—Pb(2)—O(12)	82.4 (6)	O(21)—P(2)—C(21)	107.5 (5)
O(22)—Pb(2)—O(21)	158.6 (5)	Pb(1)—O(13)—P(1)	87.4 (11)
O(13)—P(1)—O(11)	111.6 (1)	Pb(1)—O(11)—P(1)	126.4 (1)
O(13)—P(1)—O(12)	101.2 (1)	Pb(1)—O(11)—P(1)	132.1 (1)
O(13)—P(1)—C(11)	110.9 (5)	Pb(1)—O(12)—P(1)	115.8 (1)
O(22)—P(2)—O(23)	111.7 (5)	Pb(1)—O(22)—P(2)	116.6 (9)
O(22)—P(2)—O(21)	112.9 (5)	Pb(1)—O(23)—P(2)	149.9 (1)
O(22)—P(2)—C(21)	106.9 (5)	Pb(2)—O(21)—P(2)	104.4 (9)
O(11)—Pb(1)—O(12)	84.2 (6)	Pb(2)—O(21)—P(2)	144.8 (1)
O(11)—Pb(1)—O(22)	84.4 (5)	Pb(2)—O(12)—P(1)	135.9 (1)
O(11)—Pb(1)—O(23)	79.0 (7)	Pb(2)—O(13)—P(1)	136.8 (1)
O(11)—Pb(1)—O(12)	155.4 (5)	Pb(2)—O(22)—P(2)	139.4 (1)
O(22)—Pb(1)—O(23)	145.8 (4)	Pb(2)—O(23)—P(2)	89.0 (8)

3. Results and discussion

3.1. *Thermal study*

TGA and DTA curves for $Pb(O_3PC_6H_5)$ are shown in Fig. 2. There are five endotherms and one exotherm. Initially, there is an endotherm centered at 638 K, without an associated weight loss that is due to a phase transition. This structural change is currently under investigation through a thermodiffractometric study and will be reported elsewhere. At ~753 K an exotherm is observed with an important weight loss, which is due to the combustion of the organic matter. This effect is followed by two endotherms centered at 813 and 838 K, which results in the loss of all organic matter. The determined overall weight loss is 20.7%, which agrees fairly well with the theoretical weight loss of 19.0% for the decomposition of $Pb(O_3PC_6H_5)$ to $Pb_2P_2O_7$. However, the powder pattern of the sample heated at 873 K shows amorphous humps in the pattern and only a few minor Bragg peaks. There are two endotherms centered at 1083 and 1093 K, with no associated weight

losses which are due to the phase transition to crystalline $Pb_2P_2O_7$. The powder pattern of the sample heated at 1173 K matches that published by this compound in the PDF database (no. 13-0273). Lead pyrophosphate is not stable at higher temperatures as the sample heated at 1273 K starts to develop peaks of $Pb_5P_4O_{15}$, which is due to the release of P_2O_5. $Pb_5P_4O_{15}$ was identified through its published powder diffraction patterns, PDF no. 25-0452.

3.2. *Structural study*

Dispersing the sample to minimize the preferred orientation is a very important prior step in the *ab initio* procedure for lamellar compounds. It helps in two stages. First, in the indexing process, as very low-intensity peaks that are not observed when the sample is oriented, but become evident when the sample is disoriented. Second, it is also very helpful in the structural solution step as the structure factors are much less biased. It is interesting to emphasize that, with the method described above, we can slightly press to achieve a flat surface sample without increasing the preferred orientation too much. We have used the March–Dollase method to correct the preferred orientation effects (March, 1932; Dollase, 1986). This formulation is appropriate for plate-shaped microcrystals in Bragg–Brentano geometry, giving a correction factor lower than one. To estimate the effect of preferred orientation, with and without spherical particles of silica, another experiment with a sample without silica (and loaded in the same conditions) was carried out. The March–Dollases's parameter for the sample with silica was 0.868(2), while in the second case the refined parameter was far from unity, 0.570(2). This very strong preferred orientation (evidenced by the low value of this parameter) causes a drastic modification in the experimental pattern, making unsuitable the *ab initio* structure determination from powder data. The pattern of the disordered sample showed a feasible value of the March–Dollase's parameter, allowing the structure determination to be successful.

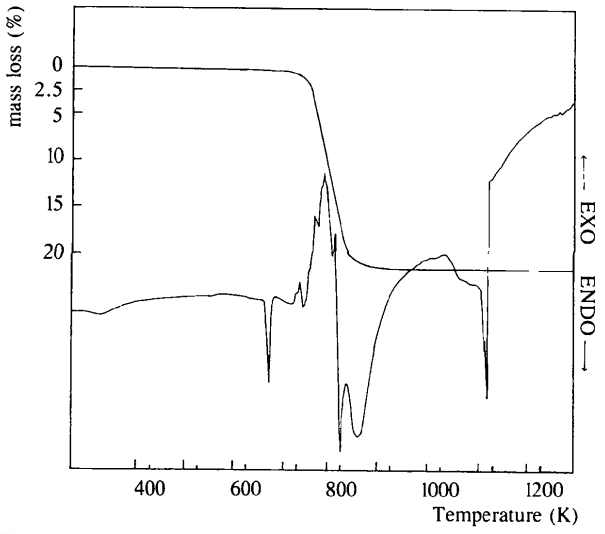

Fig. 2. DTA and TGA curves for $Pb(O_3PC_6H_5)$.

The structure of $Pb(O_3PC_6H_5)$ contains 22 atoms in the asymmetric part of the unit cell, all in general positions. Hence, there are 66 refined positional parameters. It is important to point out that this complex structure has been fully determined with medium resolution data with the help of soft constraints. The very important amount of chemical information derived in previous structural studies can be used in the way of soft/hard constraints. The geometries of the tetrahedral phosphonate groups, CPO_3, and those of the planar phenyl rings, C_6H_5, are very well known.

The crystal structure contains two crystallographically independent Pb atoms. Their environments consist of six O atoms which define two irregular polyhedra. The Pb—O bond distances range between 2.30 and 3.00 Å. This irregular coordination is due to the inert pair of Pb^{2+} cations. In these two cases the polyhedron defined by the six O atoms has a cavity where the lone pair is located (Fig. 3), resulting in an 'umbrella' coordination. The two crystallographically independent phosphonate groups are tetrahedral with P—O bonds ~1.53 Å and P—C ≃1.80 Å.

All O atoms are three-coordinated and are bonded to one phosphorus and two leads. The PbO_6 units are bonded together by sharing edges as shown in Fig. 3. A PbO_6 unit is bonded to one crystallographically equivalent PbO_6 (related by the inversion center) and two crystallographically independent PbO_6 units. Pb atoms are bonded to four oxygens of different phosphonate groups (by sharing a corner) and two oxygens of the same phosphonate (by sharing an edge). This link generates an inorganic bidimensional layer (in the crystallographic plane *bc*). The inert pairs and organic groups point to the interlamellar space (approximately in the *a* axis direction), as seen in Fig. 4.

The three-dimensional structure of this phosphonate is lamellar with only van der Waals interactions between the organic bilayers (Fig. 4). It is important to underline that the phenyl groups are tilted out to each other in order to accommodate the lone pairs.

A close inspection of the data given in Table 3

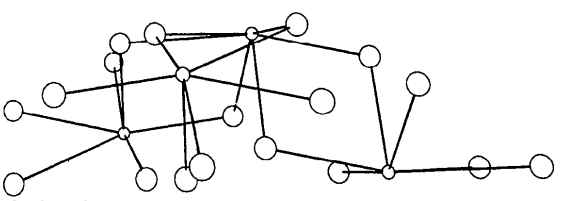

Fig. 3. Coordination environment of the Pb atoms in $Pb(O_3PC_6H_5)$.

revealed that, for example, the independent Pb atoms are almost related by the symmetry operation $x, \frac{1}{2}+y, \frac{1}{2}+z$. The same symmetry operation relates other sets of atoms. Although very low R factors are obtained, this could be attributed to the manipulation of too many variables allowed by $P\bar{1}$ with two independent molecules. To corroborate that the reported structure is triclinic and that higher symmetry is not present we carried out a MAS NMR study. If two signals are detected in the ^{31}P NMR spectrum, then triclinic symmetry is ensured. On the other hand, if the structure has higher symmetry only one ^{31}P resonance should be present.

^{31}P MAS NMR spectra of $Pb(O_3PC_6H_5)$ recorded at different experimental conditions are shown in Fig. 5. The ^{31}P MAS spectrum, recorded at 4 kHz (Fig. 5*a*), is composed of a set of lines associated with the sample spin. Although the peaks are broad, splitting of the bands is not evident in these conditions. In the CP-MAS spectrum of a sample spun at 4 kHz (Fig. 5*b*) the experimental resolution increases as a consequence of the elimination of H—P dipolar interactions. In particular, two lines are resolved in each side band, which correspond to signals with isotropic chemical shift values of 10.6 and 9.3 p.p.m. The fitting of the experimental envelope with two components is very good, indicating that both tetrahedra of phosphorus exhibit similar axial distortions (anisotropies $\Delta\delta = 66$ and 67 p.p.m.) and the same symmetry ($\eta = 0.3$). The line width of the signal at 9.3 p.p.m. is slightly broader than that of 10.6 p.p.m., indicating that residual interactions are still present. For this spectrum, the integrated intensities of the two components are 46 and 54%, respectively.

When the sample is spinning at 14 kHz, the separation of the side bands in the MAS spectrum (Fig. 5*c*) is strongly increased. This considerably reduces the number of side bands. Moreover, the experimental resolution is higher than that in the spectrum recorded at 4 kHz (Fig. 5*a*). This allows clear splitting of the two components already resolved in CP-MAS experiments. Integrated relative intensities of the components are not affected by dipolar interactions in MAS experiments. The MAS spectrum recorded at 14 kHz with the corresponding fit is shown in Fig. 6. From this fit it is confirmed that the two P environments exhibit the same multiplicity in the unit cell. Although the maximum intensity of the signal at 10.6 p.p.m. is higher than that of the signal at 9.3 p.p.m, the integrated intensity of the two bands is 50%. The peak at 9.3 p.p.m. has a smaller maximum intensity, because it is slightly broader.

The use of MAS and CP-MAS techniques reduces dipolar interactions and averages chemical shift anisotropies. However, the total elimination of dipolar interactions requires the rotation of the sample at frequencies higher than 8 kHz. The analysis of the local environment of the P atoms requires the use of low spinning rates and estimation of relative intensities in the use of high spinning rates. The observation of two

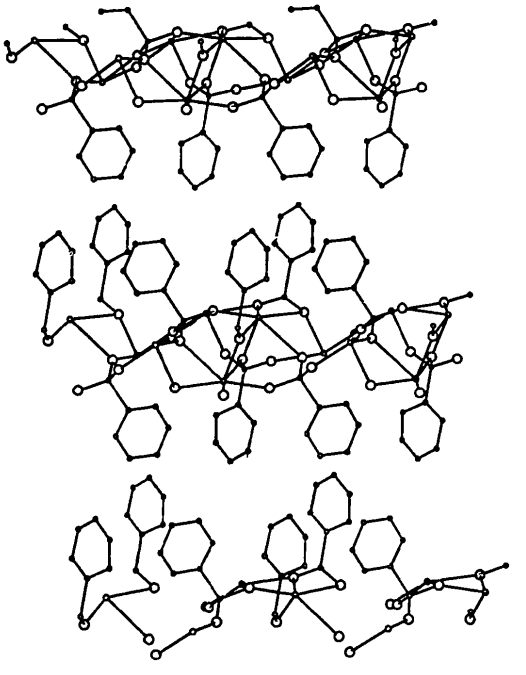

Fig. 4. Three-dimensional structure of $Pb(O_3PC_6H_5)$ showing the lamellar arrangement.

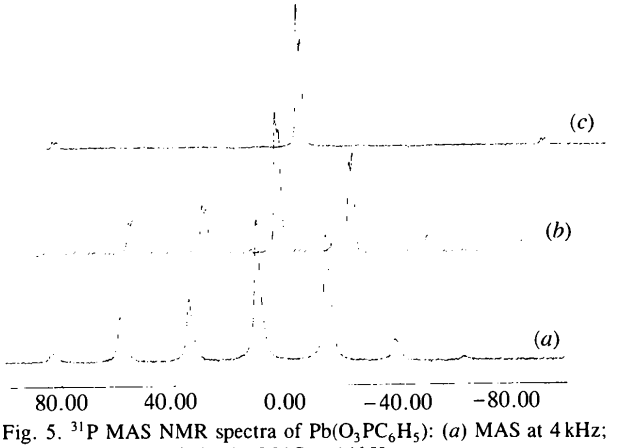

Fig. 5. ^{31}P MAS NMR spectra of $Pb(O_3PC_6H_5)$: (*a*) MAS at 4 kHz; (*b*) CP-MAS at 4 kHz; (*c*) MAS at 14 kHz.

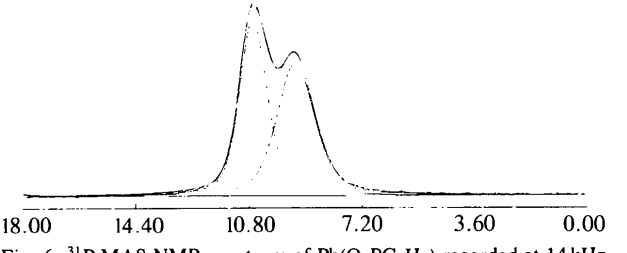

Fig. 6. ^{31}P MAS NMR spectrum of $Pb(O_3PC_6H_5)$ recorded at 14 kHz with the fit of the two components.

close ^{31}P peaks with the same multiplicity in the MAS NMR spectrum of $Pb(O_3PC_6H_5)$ confirms the existence of two different environments for P atoms in the unit cell. Hence, the triclinic symmetry of this phosphonate is guaranteed.

We thank the critical reading of the manuscript and helpful comments of Drs Clearfield and Poojary from Texas A & M University. This work was supported by CICYT research grant PB 93/1245 of Ministerio de Educación y Ciencia, Spain.

References

Alberti, G., Casciola, R., Palombari, R. & Peraio, A. (1992). *Solid State Ion.* **58**, 339-344.

Alberti, G., Costantino, U. & Giovagnotti, M. L. L. (1979). *J. Chromatogr.* **180**, 45-50.

Boultif, A. & Loüer, D. (1991). *J. Appl. Cryst.* **24**, 987-993.

Cabeza, A. (1995). PhD. Thesis. Universidad de Malaga, Spain.

Cao, G. & Mallouk, T. E. (1991). *Inorg. Chem.* **30**, 1438-1441.

Cao, G., Lee, H., Lynch, V. M. & Mallouk, T. E. (1988). *Inorg. Chem.* **27**, 2781-2785.

Cao, G., Lynch, V. M., Swinnea, J. S. & Mallouk, T. E. (1990). *Inorg. Chem.* **29**, 2112-2117.

Cheetham, A. K. (1993). *The Rietveld Method*, edited by R. A. Young, pp. 276-292. Oxford University Press.

Cheng, S. & Clearfield, A. (1986). *Appl. Catal.* **26**, 91-98.

Clearfield, A. & Smith, G. D. (1969). *Inorg. Chem.* **8**, 431-436.

Cunningham, D., Hennelly, P. J. D. & Deeney, T. (1979). *Inorg. Chim. Acta*, **27**, 95-102.

Dines, M. B. & Griffith, P. C. (1983). *Polyhedron*, **2**, 607-611.

Dollase, W. A. (1986). *J. Appl. Cryst.* **19**, 267-272.

Johnson, J. W., Jacobson, A. J., Butler, W. M., Rosenthal, S. E., Brody, J. F. & Lewandowski, J. T. (1989). *J. Am. Chem. Soc.* **111**, 381-383.

Kullberg, L. H. & Clearfield, A. (1989). *Solvent Extr. Ion Exch.* **1**, 527-540.

Larson, A. C. & Von Dreele, R. B. (1987). Report No. LA-UR-86-748. Los Alamos. National Laboratory, New Mexico, USA.

Le Bail, A., Duroy, H. & Fourquet, J. L. (1988). *Mat. Res. Bull.* **23**, 447-452.

Le Bideau, J. L., Payen, C., Palvadeau, P. & Bujoli, B. (1994). *Inorg. Chem.* **33**, 4885-4890.

March, A. (1932). *Z. Kristallogr.* **81**, 285-297.

Martin, K., Squattrito, P. J. & Clearfield, A. (1989). *Inorg. Chem. Acta*, **155**, 7-9.

Morris, M. C., McMurdie, H. F., Evans, E. H., Paretzkin, B., deGroot, J. H., Newberry, R., Pyrros, N. P., Hubbard, C. R. & Carmel, S. (1977). *Natl. Bur. Stand. (U.S.) Monogr.* **25**(14), 1-5.

Poojary, D. M., Grohol, D. & Clearfield, A. (1995). *Angew. Chem.* **34**, 13-14, 1508-1510.

Poojary, D. M., Hu, H., Campbell III, F. L. & Clearfield, A. (1993). *Acta Cryst.* B**49**, 996-1001.

Poojary, D. M., Zhang, B., Cabeza, A., Aranda, M. A. G., Brugue, S. & Clearfield, A. (1996). *J. Mater. Chem.* **5**, 639-644.

Poojary, D. M., Zhang, B. L. & Clearfield, A. (1994). *Angew. Chem.* **33**, 22, 2324-2326.

Rietveld, H. M. (1969). *J. Appl. Cryst.* **2**, 65-71.

Rudolf, P. R., Saldarriaga, C. & Clearfield, A. (1986). *J. Phys. Chem.* **90**, 6122-6125.

Segawa, K., Sugiyama, A. & Kurusu, Y. (1990). *Chem. Microporous Cryst.* **73**, 26-29.

Sheldrick, G. M. (1985). *SHELXS86. Program for the Solution of Crystal Structures.* University of Göttingen, Germany.

Smith, G. S. & Snyder, R. L. (1979). *J. Appl. Cryst.* **12**, 60-65.

Thompson, M. E. (1994). *Chem. Mater.* **6**, 1168-1175.

Troup, J. M. & Clearfield, A. (1977). *Inorg. Chem.* **16**, 3311-3314.

Werner, P. E., Eriksson, L. & Westdahl, M. (1985). *J. Appl. Cryst.* **18**, 367-370.

Wolff, P. M. (1968). *J. Appl. Cryst.* **1**, 108-113.

Zhang, Y., Scott, K. J. & Clearfield, A. (1993). *Chem. Mater.* **5**, 495-499.